THE JOURNAL OF PHYSICAL CHEMISTRY B

Article

pubs.acs.org/JPCB

Binding Kinetics and Affinities of Heterodimeric versus Homodimeric HIV-1 Reverse Transcriptase on DNA−DNA Substrates at the Single-Molecule Level

Ryan A. Marko,[†] Hsiao-Wei Liu,*[,†] Christopher J. Ablenas,[§] Maryam Ehteshami,[‡] Matthias Götte,*[,‡,§,∥] and Gonzalo Cosa*[,†]

[†]Department of Chemistry and Center for Self Assembled Chemical Structures (CSACS/CRMAA), McGill University, 801 Sherbrooke Street West, Montreal, QC, H3A 0B8, Canada

[‡]Department of Microbiology and Immunology, McGill University, 3775 University Street, Montreal, QC, H3A 2B4, Canada

[§]Department of Biochemistry, McGill University, 3655 Promenade Sir William Osler, Montreal, QC, H3G 1Y6, Canada

[∥]Department of Medicine, McGill University, 3655 Promenade Sir William Osler, Montreal, QC, H3G 1Y6, Canada

Supporting Information

ABSTRACT: During viral replication, HIV-1 reverse transcriptase (RT) plays a pivotal role in converting genomic RNA into proviral DNA. While the biologically relevant form of RT is the p66−p51 heterodimer, two recombinant homodimer forms of RT, p66−p66 and p51−p51, are also catalytically active. Here we investigate the binding of the three RT isoforms to a fluorescently labeled 19/50-nucleotide primer/template DNA duplex by exploiting single-molecule protein-induced fluorescence enhancement (SM-PIFE). PIFE, which does not require labeling of the protein, allows us to directly visualize the binding/unbinding of RT to a double-stranded DNA substrate. We provide values for the association and dissociation rate constants of the RT homodimers p66−p66 and p51−p51 with a double-stranded DNA substrate and compare those to the values recorded for the RT heterodimer p66−p51. We also report values for the equilibrium dissociation constant for the three isoforms. Our data reveal great similarities in the intrinsic binding affinities of p66−p51 and p66−p66, with characteristic K_d values in the nanomolar range, much smaller (50−100-fold) than that of p51−p51. Our data also show discrepancies in the association/dissociation dynamics among the three dimeric RT isoforms. Our results further show that the apparent binding affinity of p51−p51 for its DNA substrate is to a great extent time-dependent when compared to that of p66−p66 and p66−p51, and is more likely determined by the dimer dissociation into its constituent monomers rather than the intrinsic binding affinity of dimeric RT.

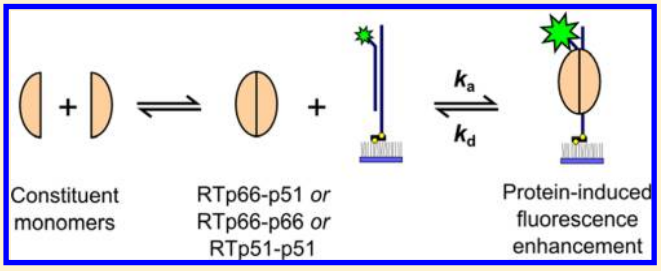

1. INTRODUCTION

During human immunodeficiency virus type 1 (HIV-1) replication, reverse transcriptase (RT) is responsible for an obligatory step involving the conversion of single-stranded genomic RNA into double-stranded proviral DNA. RT isolated from virions is a heterodimeric protein consisting of two polypeptide chains, a 66 kDa subunit (p66) and a 51 kDa subunit (p51).[1,2] The p66 subunit comprises a polymerase and a ribonuclease (RNase) H domain, with a connection domain linking the two catalytically active sites. The RNase H domain cleaves the RNA moiety of RNA/DNA replication intermediates, which is likewise essentially required for proviral DNA synthesis.[3] The p51 subunit, processed by proteolytic cleavage of p66 during viral maturation, corresponds to the N-terminus of the polymerase domain and lacks the RNase H domain. Although the two subunits are encoded by the same gene, distinct foldings result in an asymmetric dimeric structure.[4,5] Consequently, the p51 subunit is catalytically incompetent; its role is limited to stabilizing the p66 subunit and it also provides contacts to the bound nucleic acid substrate. However, the nucleic acid binding channel is primarily formed by elements of the large p66 subunit.[3,6]

Sluis-Cremer et al. have proposed two possible mechanisms for HIV-1 RT heterodimerization during viral maturation.[7] In the sequential model, RT initially exists as p66−p66 homodimers, after being processed from the Gag-Pol polyprotein precursor by the viral protease. Subsequent proteolytic cleavage of one subunit of the p66−p66 homodimer removes the C-terminal (p15) RNase H domain, yielding the p66−p51 heterodimer. Alternatively, in the concerted model, viral protease excises the Gag-Pol polyprotein precursor into separate p66 and p51 monomers, followed by rapid heterodimerization of p66

Special Issue: Paul F. Barbara Memorial Issue

Received: August 31, 2012
Revised: December 25, 2012
Published: January 10, 2013

and p51. To test these models, Sluis-Cremer et al. expressed precursors containing the L234A mutation, known to impair p66−p66 dimerization.[8,9] The formation of processed p66 accompanied by little p51 provides support for the sequential processing pathway. Here, the formation of p66−p51 occurs via a p66−p66 homodimer intermediate and yields practically equivalent amounts of p66 and p51 subunits in HIV-1 virions.[2,10]

In addition to heterodimeric p66−p51, active homodimeric forms of HIV-1 RT p66−p66 and p51−p51 have been characterized.[11−13] Biochemical studies have shown that p66−p66 homodimers possess polymerase and RNase H activity comparable to their heterodimeric counterparts.[2,14,15] In sharp contrast, several groups have reported that p51−p51 homodimers possess modest to negligible DNA polymerase activity.[11,14,16−20] However, little information is available on the binding of these dimers to their nucleic acid substrates.

Single-molecule techniques are ideally positioned to unravel the biochemical mechanism and biological function of protein−nucleic acid interactions. Whereas static and dynamic protein−nucleic acid interactions have mostly been studied using single-molecule fluorescence resonance energy transfer (SM-FRET), this technique often necessitates site-specific fluorescent labeling of protein and/or nucleic acid species.[21−27] For example, the growth of RecA filaments along single-stranded DNA (ssDNA) can be monitored solely by employing ssDNA labeled with Cy3 and Cy5 fluorescent dyes.[28] In contrast, in order to observe FRET changes induced by the association of heterodimeric HIV-1 RT with its nucleic acid substrates, both enzyme and substrate have been fluorescently labeled.[24] Introduction of protein labeling to homomultimer systems (e.g., RecA filaments or homodimeric RT) is, however, problematic due to the possibility that multiple fluorescently tagged subunits are complexed with singly-labeled DNA substrates, making it challenging to interpret SM-FRET signals.

Here, we report a single-molecule protein-induced fluorescence enhancement (SM-PIFE) assay designed to directly visualize binding of RT to DNA−DNA primer-template with no protein labeling requirement. In PIFE, protein binding to, e.g., double-stranded DNA leads to a decrease in the nonradiative decay pathway of a DNA-tethered fluorophore by reducing the weight of internal conversion in the rate of relaxation of the photoexcited dye. This reduction is concomitant with an increase in emission intensity.[29,30] The PIFE assay has facilitated the understanding of protein−nucleic acid interactions in biological systems such as the conformational change of bacteriophage T7 DNA polymerase during DNA synthesis, the translocation of a DNA helicase, and the formation of RecA filaments along their DNA substrates.[29,30]

Employing SM-PIFE, here we investigate both the binding affinity and kinetics of HIV-1 RTp66−p51 heterodimer versus RTp66−p66 or RTp51−p51 homodimers when exposed to their DNA−DNA substrates. We directly visualize the binding/unbinding process of RT on a DNA−DNA substrate by following RT-induced fluorescence fluctuations. The binding parameters derived from the SM-PIFE data reveal great similarities in the intrinsic binding affinities of RTp66−p51 and RTp66−p66 to the DNA susbtrate, with characteristic K_d values in the nanomolar range, much smaller (50−100-fold) than that measured for p51−p51. The binding parameters also show discrepancies in the association/dissociation kinetics among the three dimeric RT isoforms.

2. EXPERIMENTAL SECTION

Protein Expression and Purification. Recombinant HIV-1 RTp66−p51 heterodimers were expressed and purified as previously described.[12] M15 competent cells were transformed with the pRT6Hpr$^-$ plasmid, which allows for the expression of RTp66 in the absence of HIV-1 protease. The lack of protease allows for the expression of RTp66 without a subsequent cleavage to generate RTp51. The remainder of the purification method was identical to that of RTp66−p51 heterodimers. The RTp51 harboring a N-terminal glutathione S-transferase (GST) tag was generated separately by transforming BL21DE3 *E. coli* cells with the pGEXp51 vector. Induced RTp51 was purified through a GST column, with increasing concentrations of glutathione. Purified RT (p66−p51, p66, and p51) was then stored at high concentrations (100−300 μM) in RT buffer (50 mM Tris−HCl pH 8.0, 50 mM NaCl) with 50% glycerol at −20 or −80 °C.

Preparation of Primer/Template Strands. The DNA sequences used in this work (primer: 5′-TTTTATATCTATAGCGCGC-3′; template: 5′-ATTAGATTAGCCCTTCCAGTGCGCGCTATAGATATAAAAAGTGGCGTGGC-3′) were acquired from Integrated DNA Technologies (Coralville, IA). The strands were purified using HPLC. The 3′-terminus of the primer strand was conjugated to a Cy3 dye via phosphoramidite chemistry. In order to enable surface immobilization of the DNA duplex, the 3′-terminus of the template strand was attached to a biotin moiety via a C6 linker, which was in turn coupled to the 3′OH of the deoxyribose. The Cy3-biotinylated primer-template duplexes were prepared by mixing the primer strands and the template strands in annealing buffer (50 mM Tris−HCl and 40 mM NaCl, pH 8.0) at a ratio of 2:1. The mixture was then incubated in a thermal cycler (Eppendorf, Mississauga, Canada) at 95 °C for 2 min followed by a gradual cooling step of 2 °C/min to 25 °C. Duplex formation of the primer and template strands was confirmed using 10% native polyacrylamide gel electrophoresis.

Single-Molecule Sample Preparation and Imaging. In order to prevent nonspecific adsorption of biomolecules onto the glass surface, coverslips were functionalized prior to use with a mixture of poly(ethylene glycol) succinimidyl valerate, MW 5000 (mPEG-SVA), and biotin-PEG-SVA (Laysan Bio, Inc.) at a ratio of 99/1 (w/w), following a previously described protocol.[31] The surface was incubated with 10 μL of 0.2 mg/mL streptavidin solution (Sigma Aldrich, St. Louis, MO) for 10 min followed by ∼20 μL of 100 pM biotinylated Cy3-primer-template duplexes to achieve a good surface density (∼300 fluorescent spots per 30 μm × 30 μm region). Unbound duplexes were then flushed out with imaging buffer (50 mM Tris−HCl pH 8.0, 40 mM NaCl, 6 mM $MgCl_2$). RT solutions ranging from 2 to 300 nM were prepared in the otherwise identical imaging buffer. Experiments with RTp51 were conducted at much higher concentration to promote homodimer formation. The non-nucleoside RT inhibitor (NNRTI) efavirenz (EFZ), known to enhance the dimer formation of RT, was also employed in studies with RTp51. RTp51 (1.46 μM) was initially incubated with efavirenz (72 μM) in imaging buffer for 16 h at 4 °C. Immediately prior to image acquisition, RTp51 and efavirenz were diluted to final concentrations of 1.4 and 70 μM, respectively, upon the addition of oxygen scavenging and triplet quenching components (see below). For monitoring the time-dependent dissociation of homodimeric RT, we diluted the protein from concentrated stock solutions (∼200−300 μM) to

dx.doi.org/10.1021/jp308674g | J. Phys. Chem. B 2013, 117, 4560−4567

58 nM (RTp66) or 1.46 μM (RTp51) in imaging buffer and incubated the samples for various time intervals, at 4 °C. The protein was further diluted to a final concentration of 50 nM (RTp66) or 1.4 μM (RTp51) upon the addition of oxygen scavenging and triplet-state quenching components immediately before being introduced to the imaging chamber.

Imaging chambers (~8 μL) were constructed by pressing a polycarbonate film with an adhesive gasket (Grace Bio-Lab, Bend, OR) onto a PEG-coated coverslip. Two silicone connectors (Grace Bio-Lab, Bend, OR) were glued onto the predrilled holes of the film and served as inlet and outlet ports.[32] Prior to image acquisition, tubing was inserted into the inlet port, connecting the chamber to a syringe containing the RT solution that was then placed on a syringe pump. Image acquisition began simultaneously as the pump started to flow the RT solution at 10 μL/min into the chamber to replace the pre-existing imaging buffer. Due to the dead volume of the flow tubing, the RT-induced fluorescence enhancement of Cy3 on primer-template duplexes was observed ~1 min after initiating RT flow.[33] To delay the photobleaching of Cy3, all the solutions employed in single-molecule imaging experiments contained an oxygen scavenging component containing 0.1 mg/mL glucose oxidase (Sigma Aldrich, St. Louis, MO), 0.02 mg/mL catalase (Sigma Aldrich, St. Louis, MO), and 3% (w/w) β-D-glucose (Sigma Aldrich, St. Louis, MO) combined with a triplet-state quenching component of 143 mM β-mercaptoethanol (Sigma Aldrich, St. Louis, MO).

The fluorescence imaging of surface-anchored primer-template duplexes was conducted using an objective-type total internal reflection fluorescence (TIRF) microscope (Olympus IX-71 inverted microscope) in conjunction with a back-illuminated electron multiplying charge coupled device (EM-CCD) detector (Cascade II:512; Roper Scientific, Tucson, AZ). Excitation was carried out with a diode-pumped solid-state green laser (532 nm cw from Crystal Laser, Reno, NV) with a power output of ca. 10 mW measured from the objective in the wide field mode. The excitation was directed by a dichroic mirror (Z532rdc, Chroma Technology, Rockingham, VA) to an oil immersion microscope objective (60× PlanApo N; N.A. = 1.45; Olympus). The laser beam was focused onto the back focal plane of the objective using a TIRF illumination module (IX2-RFAEVA-2, Olympus) to yield an evanescent wave excitation at the glass–water interface. The fluorescence of the primer-template duplexes was collected by the objective and imaged onto the EM-CCD detector. A bandpass filter (HQ 590/70, Chroma Technology, Rockingham, VA) was placed in front of the EM-CCD detector to remove the scattered light. An additional magnification of 2× was introduced by a relay lens located between the camera and the microscope, resulting in pixels of ca. 135 nm. Images consisted of ca. 70 μm × 70 μm regions. The camera was controlled using Image-Pro Plus 5.1 (Media Cybernetics), capturing 8-bit 512 × 512 pixel images with a conversion gain of 3 and a multiplication gain of 4095. The exposure time per frame ranged from 100 to 280 ms, and a total of 1000 to 1500 frames were acquired in each measurement. Fluorescence intensity–time trajectories of individual molecules were extracted from the videos using a self-written algorithm in IDL and Matlab.

3. RESULTS AND DISCUSSION

Binding of p66–p51 Heterodimers with Cy3-Primer-Template Substrates. We first investigated whether PIFE would be applicable to monitor the binding of HIV-1 RTp66–p51 to surface-immobilized Cy3-primer-template, hereafter noted as Cy3-P-T. To ensure saturation binding of RTp66–p51 to Cy3-P-T, large enzyme concentrations, ca. 300 nM, were employed. A diagram of the assay used for SM-PIFE measurements is depicted in Figure 1A. We employed a flow system allowing for

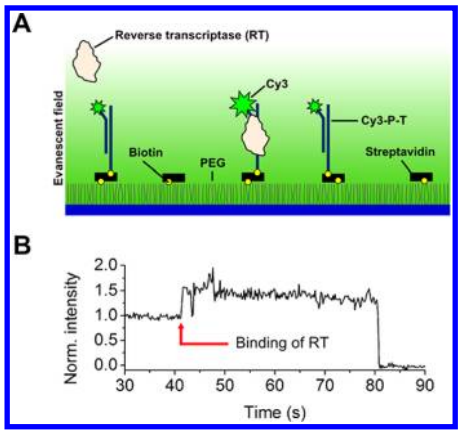

Figure 1. A cartoon illustrating the single-molecule protein-induced fluorescence enhancement (SM-PIFE) assay for detecting RT binding to a DNA–DNA substrate. (A) A total internal reflection fluorescence microscopy setup combined with surface-immobilized Cy3-labeled primer-template (Cy3-P-T) was employed for our SM-PIFE measurements. (B) A representative normalized intensity–time trajectory of Cy3-P-T acquired while 300 nM RTp66–p51 flowed into the imaging chamber shows the binding of RT to Cy3-P-T and the induced fluorescence enhancement.

the rapid delivery of RT into the chamber where the buffer solution was readily switched from no RT to 300 nM RTp66–p51 (see the Experimental Section). During the buffer exchange, images were acquired over time wherefrom the fluorescence intensity of hundreds of individual Cy3-P-T molecules were simultaneously recorded in order to extract their intensity–time trajectories. As shown in Figure 1B, we observed a ca. 30% fluorescence enhancement for individual Cy3 due to RT binding. For RT concentrations ≥50 nM, fluorescence enhancement occurred synchronously among the majority of molecules recorded, supporting the notion that the observed intensity increases are due to RT binding (Figure S1, Supporting Information). We observed no fluorescence enhancement in control experiments acquired flowing solutions with no RT but under otherwise identical conditions (Figure S2, Supporting Information). We therefore assign the baseline intensity and the elevated intensity in Figure 1B to an RT-unbound state (off-state) and an RT-bound state (on-state), respectively.

Since the nucleic acid binding cleft of RTp66–p51 can accommodate a nucleic acid duplex of 18–22 base-pairs between both active sites,[34] we expected to observe a 1:1 complex composed of RTp66–p51 and Cy3-P-T (the duplex region in our single molecule substrate consists of 19 base pairs). However, an electrophoretic mobility shift assay (EMSA) also revealed the formation of higher-order complexes for RTp66–p51 concentrations ≥300 nM and RTp66–p51/Cy3-P-T molar ratios ≥4 (Figure S3, Supporting Information). It is plausible that the aggregated RT/Cy3-P-T complex involves RT oligomers, as previously observed in a chemical cross-linking assay.[35] To avoid PIFE effects due to aggregated RT, the remaining single-molecule experiments were acquired with HIV-1 RT concentrations ≤50 nM.

dx.doi.org/10.1021/jp308674g | J. Phys. Chem. B 2013, 117, 4560–4567

To gain insight into the affinity and kinetics of RTp66−p51 binding to Cy3-P-T, we conducted SM-PIFE studies at different RTp66−p51 concentrations. Figure 2A shows two

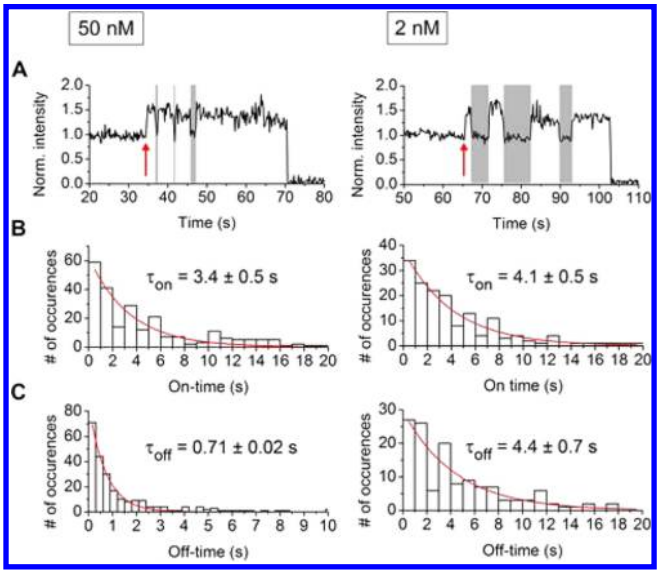

Figure 2. Monitoring RT binding/unbinding kinetics in the presence of 50 nM (left) and 2 nM RTp66−p51 (right). Panel A depicts single-molecule intensity−time trajectories of Cy3-P-T at two RTp66−p51 concentrations. Each trajectory was normalized to its average intensity during the initial period when RT was not present. The red arrows correspond to the first RT binding event, and the shaded areas correspond to the off-states where Cy3-P-T is unbound to RT. Panels B and C show on- and off-time histograms, respectively, constructed on the basis of at least 60 single-molecule intensity−time trajectories. Also shown are the fittings (red) with a single exponential decay function.

intensity−time trajectories acquired with 50 and 2 nM RT. After the introduction of RTp66−p51 into the imaging chamber, the intensity−time trajectories fluctuated between the elevated (on) and baseline (off) levels, indicating that P-T switched between the RT-bound and RT-unbound states, respectively. The duration of the on-state was independent of RTp66−p51 concentration (consistent with a protein dissociation rate which is first order in the concentration of RT/Cy3-P-T complex). In contrast, the duration of the off-state was shorter with increasing RTp66−p51 concentration; see shaded areas in Figure 2A (this result is consistent with a second-order process, first order in both [RT] and [Cy3-P-T]). The association and dissociation dynamics follow the elementary reaction steps shown in eq 1:

$$\mathrm{RT} + \text{Cy3-P-T} \underset{k_d}{\overset{k_a}{\rightleftharpoons}} \mathrm{RT/Cy3\text{-}P\text{-}T} \quad (1)$$

In order to gain a quantitative insight on the rate constants involved in the association (k_a) and dissociation (k_d) processes, we conducted further analysis of the intensity−time trajectories using a hidden Markov model based on a three-state system[36] (Supporting Information, Figure S4) wherefrom the off and on interval durations could be extracted.[37] We next constructed histograms of the durations of Cy3-P-T in the on-states and off-states (hereafter referred to as on-time and off-time, respectively) based on at least 60 molecules for each RTp66−p51 concentration. Single exponential fittings of the histograms yielded the dissociation rate constant, k_d ($1/\tau_{on}$) and the pseudo-first-order association rate constant ($1/\tau_{off}$), where [RTp66−p51] ≫ [Cy3-P-T], under our experimental conditions (see Figure 2B and C and Table 1; also see Figure S4 in the Supporting Information). We obtained values of $k_d = 0.28 \pm 0.03\ s^{-1}$

Table 1. Dissociation/Association Rate Constants and Equilibrium Dissociation Constants for the Three Dimeric RTs and Their Nucleic Acid Substrates

constant	RTp66−p51	RTp66−p66	RTp51−p51	RTp51−p51+EFZ[a]
k_a (s^{-1} M^{-1})	1.1×10^8 [b]	1.2×10^7 [b]	N/A	1.6×10^6 [b]
	$(2 \pm 1) \times 10^8$ [c]			
k_d (s^{-1})	0.28 ± 0.03[d]	0.40[d]	N/A	1.9[d]
	0.13 ± 0.01[e]			
	0.2[f]			
K_d (nM)	3.9 ± 2.9[d]	9.8[d]	N/A	440[d]
	9.33 ± 0.09[g]			
	4.7 ± 0.4[f]			

[a]Data acquired after 16 h of incubation of RTp51 with 50-fold EFZ (70 μM). [b]Data were measured by SM-PIFE under pseudo-first-order conditions, where [RT] was significantly greater than [Cy3-P-T]. The apparent association rate constants were estimated by dividing the pseudo-first-order association rate constants by the RT concentration. The value reported for RTp66−p51 was calculated using [RTp66−p51] = 2 nM (see main text). The values reported for RTp66−p66 and RTp51−p51 were calculated using [RTp66−p66] = 25 nM based on the assumption that the enzyme was fully dimerized and [RTp51−p51] = 0.49 μM based on the $K_{d,p51-p51}$ value in the presence of efavirenz (EFZ) reported by Venezia et al.[42] [c]Data on a 19/53-mer DNA−RNA primer-template reported by Kruhøfter et al. at 6 mM Mg^{2+}.[38] [d]Data were measured by SM-PIFE under pseudo-first-order conditions, where [RT] was significantly greater than [Cy3-P-T]. The value reported for RTp66−p51 represents the average ± standard deviation of three independent trials conducted at 2, 25, and 50 nM. The values reported for RTp66−p66 and RTp51−51 (with EFZ) were obtained at the same dimer concentrations as listed in entry *b* above, respectively. Experimental errors are expected to be similar to those reported for RTp66−p51. [e]Data on a 22/44-mer DNA−DNA primer-template reported by Reardon at 5 mM Mg^{2+}.[49] [f]Data on a 25/45-mer DNA−DNA primer-template reported by Kati et al. at 10 mM Mg^{2+}.[45] [g]Data on a 25/30-mer DNA−DNA primer-template reported by DeStefano et al. at 6 mM Mg^{2+}.[44]

and $k_a = 1.1 \times 10^8\ M^{-1}\ s^{-1}$, the latter being calculated from measurements conducted with 2 nM RT by dividing the pseudo-first-order rate constant obtained by [RTp66−p51]. The value of k_a we found is comparable to that of $2 \times 10^8\ M^{-1}\ s^{-1}$ obtained from stopped-flow experiments reported by Kruhøfter et al.[38] We note that, although the τ_{off} values derived from the SM-PIFE data at 25 and 50 nM RTp66−p51 were shorter than the τ_{off} obtained with 2 nM RTp66−p51, the values did not decrease in a concentration-dependent manner. The overestimated τ_{off} at higher RT concentration is due to the time resolution in our measurements, which is unable to resolve the shorter unbound events with off-times <280 ms.

Hwang et al. have demonstrated that the extent of PIFE is markedly dependent on the distance between the fluorescent dye and the protein for separations below 4 nm[29] and may be intrinsically related to the steric hindrance the protein provides.[30,39] RTp66−p51 may bind primer-template substrates in two distinct orientations with either the polymerase or RNase H domain positioned at the 3′ terminus of the primer.[40,41] As a result, one might expect each orientation to induce a different degree of fluorescence enhancement. Abbondanzieri et al. have demonstrated however that, for the DNA duplex employed in our studies, the polymerase domain of RTp66−p51 preferentially

dx.doi.org/10.1021/jp308674g | J. Phys. Chem. B 2013, 117, 4560−4567

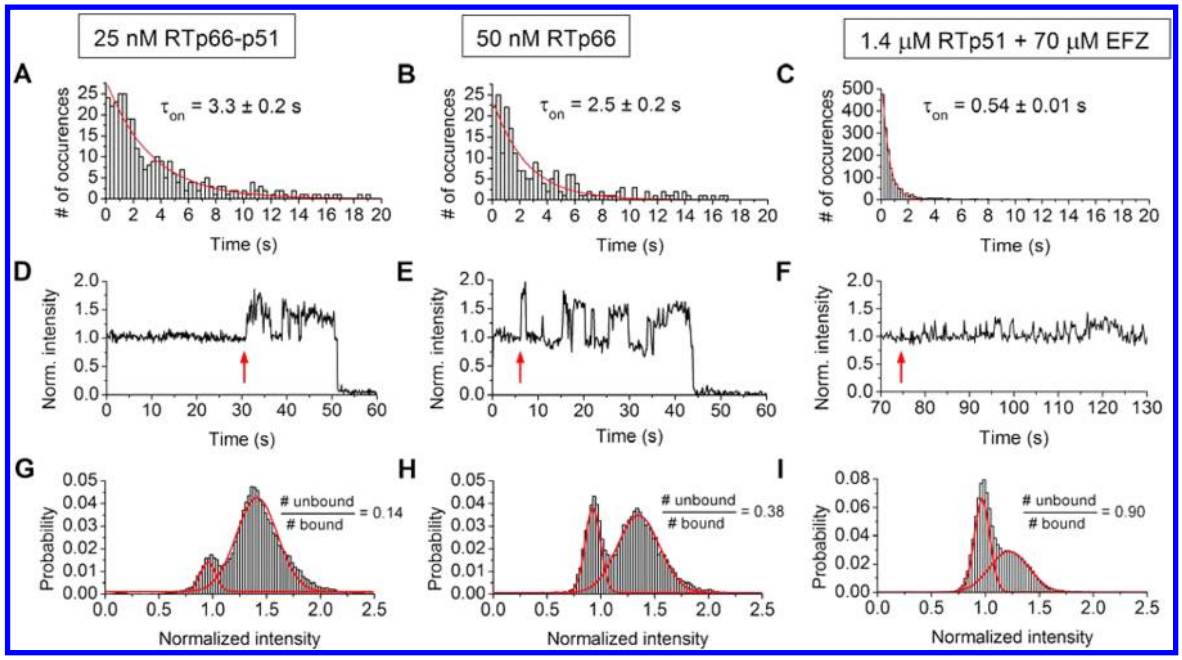

Figure 3. Binding of heterodimeric and homodimeric RT to Cy3-P-T. (A–C) Ensemble on-time histograms for Cy3-P-T in the presence of one of the three RT isoforms. Exponential fittings are also shown (red curves). (D–F) Examples of individual normalized intensity–time trajectories acquired for Cy3-P-T in the presence of one of the three RT isoforms. Each trajectory was normalized to its initial average intensity when no protein was present in the imaging chamber. Red arrows indicate the onset of the first intensity enhancement event due to RT binding. (G–I) Ensemble histograms constructed with the individual normalized intensity–time trajectories of Cy3-P-T acquired in the presence of one of the three RT isoforms. The ensemble histograms were fitted with a bimodal Gaussian distribution. The protein concentrations used in these experiments were 25 nM RTp66–p51 (left), 50 nM RTp66 (middle), and 1.4 μM RTp51 incubated with 70 μM efavirenz (EFZ) (right).

binds the 3′ termini of primers ~90% of the time.[24] On the basis of the results by Abbondanzieri et al., we are predominantly probing interactions between the polymerase active site of RTp66–p51 and Cy3 on the Cy3-P-T construct employed in our studies.

Control SM-PIFE studies performed on a Cy3-P-T with a different Cy3 labeling site (attached to the 5′ terminus of the primer rather than the 3′ terminus) yielded a similar fluorescence enhancement upon binding of RTp66–p51 (Supporting Information, Figure S6). The dominant binding mode in the latter case positions the RNase domain close to Cy3. Thus, SM-PIFE may not enable us to distinguish polymerase vs RNase domain binding, since they both gave rise to a similar enhancement. Albeit no difference may be appreciated between the binding of polymerase and RNase domains based on SM-PIFE, the two-state[36] rather than multistate intensity fluctuations observed in the Cy3-P-T trajectories in the presence of RTp66–p51 (Figures 2A and 3G) together with results from Abbondanzieri et al. support the notion that we are probing a specific binding orientation of RT. Two-state intensity fluctuations for Cy3-P-T are observed in the presence of all three RT dimers (see Figure 3 in the following section).

Binding Kinetics and Affinity for RT Heterodimer and Homodimers. In order to determine whether or not significant differences in binding affinity to Cy3-P-T exist between heterodimeric and homodimeric forms of RT, we next conducted SM-PIFE measurements with homodimeric constructs RTp66–p66 and RTp51–p51. The parameters related to the binding kinetics of the three RT dimers with Cy3-P-T are summarized in Figure 3 and Table 1. The average time required for RT to dissociate from the complexes, τ_{on} ($1/k_d$, derived from the on-time histograms in Figure 3A–C), is indicative of the stability of RT/Cy3-P-T complexes. The k_d value we obtained for RTp51–p51/Cy3-P-T (in the presence of efavirenz (EFZ), see below) was the largest among the three RT/Cy3-P-T complexes (see Table 1). A closer look at the normalized intensity–time trajectories of individual Cy3-P-T molecules in Figure 3D–F reveals faster dissociation dynamics for RTp51–p51. While the RT unbound/bound ratios of Cy3-P-T for p66–p51 and p66–p66 were within the same order of magnitude (Figure 3G,H), binding of RTp51–p51 to Cy3-P-T was scarce under the same monomer concentration (50 nM, data not shown). As we increased the RTp51 monomer concentration to 1.4 μM, the majority of Cy3-P-T remained in the unbound state, with an unbound/bound ratio of ~5; the intensity–time trajectories under this condition did not exhibit sufficient binding/unbinding events for obtaining reliable τ_{on} and τ_{off}. Only upon incubating RTp51 with 50-fold EFZ (a non-nucleoside RT inhibitor (NNRTI) known to enhance the dimer formation of RT) did the unbound/bound ratio drastically decrease to 0.9. The resulting ensemble normalized intensity histogram and on-time histogram (Figure 3C and F) indicated that binding of RTp51–p51 to Cy3-P-T is highly dynamic, characterized by 5–7-fold faster dissociation rates when compared to those of RTp66–p51 and RTp66–p66 (see Table 1).

The analysis of the intensity–time trajectories not only provides dynamic information but also may yield information on the affinity of RT, either homo- or heterodimer, for its P-T substrate. The ensemble normalized intensity histograms may provide a quantitative value for the RT unbound/bound ratio at a given RT concentration. Next, it is possible to estimate the apparent dissociation constant of RT/Cy3-P-T (K_d) according to eq 2:

$$K_d = \frac{\#\text{ of events, unbound}}{\#\text{ of events, bound}}[\text{RT}] \quad (2)$$

dx.doi.org/10.1021/jp308674g | J. Phys. Chem. B 2013, 117, 4560–4567

Table 1 lists the K_d values for RTp66−p51 and the homodimers RTp66−p66 and RTp51−p51 obtained on the basis of eq 2. Values for RTp66−p66 and RTp51−p51 (in the presence of efavirenz) are shown to be 2.5- and 112-fold larger, respectively, than those acquired for RTp66−p51 (K_d = 3.9 nM).

Critical to the analysis of the above results and those presented in the ensuing section is the consideration of the dynamic equilibrium between the RT dimer and its constituent monomers. The documented equilibrium dissociation constant for the dimer−monomer equilibrium of RTp66−p51 ($K_{d,p66-p51}$) has been reported to be 310 nM.[42] Such a large value for the dissociation constant of the heterodimer would imply that only ∼0.6% (or 13 pM) RTp66−p51 actually exists in its dimeric state under our experimental conditions (initial 2 nM RTp66−p51). In turn, such a low effective RT dimer concentration would require revising eq 2 by inserting the real dimer concentration, leading to a K_d value of ∼8 pM for the RTp66−p51/Cy3-P-T complex. We note however that, in our SM-PIFE assay, care was taken to rapidly dilute RTp66−p51 from a concentrated stock solution (∼100 μM). The dissociation kinetics of the RT heterodimer have been shown to be significantly slow, with a dimer dissociation half-life ($t_{1/2}$) of ∼48 h at 5 °C,[43] much longer than the course of our SM-PIFE measurements (∼5 min). Thus, under our conditions, all the RTp66−p51 should be fully dimerized, leading to a K_d value of 3.9 nM. This K_d value, derived on the basis of 100% heterodimeric RT, is consistent with K_d values of a few nanomolar previously reported by two independent groups using longer DNA−DNA primer-template constructs (see Table 1).[44,45]

Likewise, to calculate the K_d value of RTp51−51/Cy3-P-T with EFZ, it is necessary to estimate the amount of dimeric species in the RTp51 solution. Several analytical methods have been applied to characterize the homodimerization of RTp51, with reported $K_{d,p51-p51}$ values ranging from 230 to 670 μM. Therefore, it is not surprising that only ∼20% Cy3-P-T were bound with RTp51−p51 (at 1.4 μM monomer concentration) in our SM-PIFE measurements.[19,42] Venezia et al. further suggested that incubation of RTp51 with saturating levels of EFZ enhanced the p51 dimerization and decreased the $K_{d,p51-p51}$ to 0.37 μM.[42] Presumably, the monomer−dimer equilibrium should have been established after 16 h of incubation with EFZ. On the basis of this $K_{d,p51-p51}$ value, we obtained 0.49 μM of dimeric RTp51−p51 and a K_d value of 440 nM for RTp51−51/Cy3-P-T with EFZ (Table 1).

Binding Activities of Homodimeric RTp66−p66 and RTp51−p51 as a Function of Time. Nuclear magnetic resonance (NMR) spectroscopy studies have revealed that RTp51−p51 possesses a nucleic acid binding cleft where one p51 subunit of the homodimer adopts an open and extended structure resembling the p66 subunit of RTp66−p51.[46] On the basis of such structural similarity between RTp66−p51 and RTp51−p51 (to our knowledge, there is no structural data available for RTp66−p66), the binding affinities of homodimeric and heterodimeric RT to nucleic acid substrates are arguably comparable to one another. It is thus surprising that the K_d value of RTp51−p51 in complexation with Cy3-P-T, calculated from data in Figure 3I and listed in Table 1, is ∼50−100 fold bigger than that of RTp66−p51 and RTp66−p66. It must be emphasized that all SM-PIFE measurements were conducted rapidly to minimize the effect of RT dimer dissociation into its constituent monomers. Thus, RTp66−p66 or RTp51−p51 were diluted from a concentrated stock solution (∼200 μM), and immediately flowed into imaging chambers containing the immobilized Cy3-P-T, in an analogous manner to the aforementioned preparation of RTp66−p51 imaging studies (see also the Experimental Section for further details).

Restle et al. have reported $t_{1/2}$ values of 19 h for RTp66−p66 and 3 h for RTp51−p51 at 0 °C.[19] Therefore, it is highly plausible that the population of RT-bound states displayed in Figure 3I is due to residual RTp51−p51 dimers existing in the solution, where the RTp51 monomer/dimer equilibrium has not yet been established following rapid dilution of the concentrated stock solution. To test the above hypothesis, we incubated diluted RTp66 or RTp51 solutions, prepared from the 200 μM stock, in imaging buffer for increasing time intervals before introducing the protein solutions to Cy3-P-T in the imaging chamber. Considering that the reported dimer dissociation

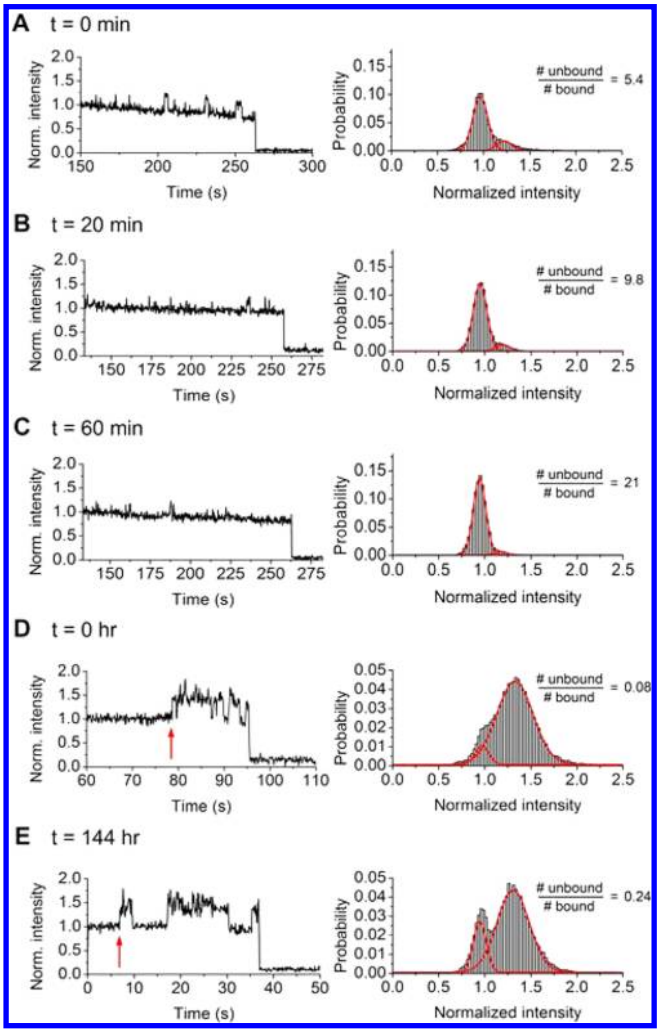

Figure 4. Intensity−time trajectories (left) and ensemble normalized intensity histograms fitted with Gaussian bimodal distributions (right) for Cy3-P-T in the presence of 1.4 μM RTp51 and 50 nM RTp66, as a function of incubation time following dilution of the RT isoforms from a concentrated (ca. 200 μM) solution. (A−C) Intensity−time trajectories and ensemble normalized intensity histograms acquired in the presence of RTp51−p51 at (A) 0 min and (B) 20 min and (C) 60 min incubation periods; trajectories are recorded 2 min after protein is flowed into chambers. (D, E) Intensity−time trajectories and ensemble normalized intensity histograms acquired in the presence of RTp66 at (D) 0 h and (E) 144 h incubation periods. Red arrows indicate the onset of the first intensity enhancement event due to RT binding; trajectories are recorded as soon as protein is flowed.

dx.doi.org/10.1021/jp308674g | J. Phys. Chem. B 2013, 117, 4560−4567

constants for RTp66−p66 and RTp51−p51 ($K_{d,p66-p66}$ and $K_{d,p51-p51}$) are a few micromolar and hundreds of micromolar, respectively,[19,42] we anticipated that the diluted RT homodimers would readily dissociate into monomers over time. Since monomeric p66 or p51 are incapable of binding to DNA primer-template substrates,[47] dimer dissociation of RT would shift the equilibrium of Cy3-P-T from the bound toward unbound states.

Following an incubation period (up to 1 h) of a diluted RTp51 (1.4 μM) at room temperature in imaging buffer prior to its inclusion in the imaging chamber, we observed a dramatic reduction in the binding affinity of RTp51−p51 for its DNA substrate, consistent with the dissociation of the homodimer into its constituent monomers within this short time window (Figure 4A and B). Attempts to perform this set of experiments with 50 nM RTp51 (whether it was diluted directly from the 200 μM stock solution or from the RTp51 (1.4 μM) with EFZ (70 μM) after 16 h incubation) failed due to the scarce binding events caused by the very rapid dissociation of RTp51. In contrast, an appreciable decrease in the RT-bound fraction of the Cy3-P-T population appeared only upon incubating diluted RTp66−p66 (50nM) for over 144 h at 4 °C (see Figure 4C and D), despite the fact that the RTp66−p66 concentration was in the nanomolar range, far below the dimerization $K_{d,p66-p66}$ value of ∼4 μM. Similar results to those of RTp66−p66 were obtained for RTp66−p51 (not shown).[42] The slow reduction in binding affinity for RTp66−p66 suggests that the rate of dissociation of RTp66−p66 into its constituent monomers is significantly smaller than the $t_{1/2}$ = 19 h reported by Restle et al.[19] In their work, Restle et al. induced the dissociation of dimers by diluting RT solutions with 20% acetonitrile. The effect of the organic solvent on promoting dimer dissociation (as suggested by Venezia et al.[43]) may account for the discrepancy in the dissociation rate values reported here and those listed in the previously published work.[19]

4. CONCLUSIONS

By using a flow system combined with the SM-PIFE approach, we have been able to investigate the binding of HIV-1 RTp66−p51 heterodimer and the two recombinant homodimers RTp66−p66 and RTp51−p51 to a DNA−DNA substrate. Binding kinetics of RT on nucleic acid substrates have typically been estimated indirectly via the amount of DNA synthesized or RNA degradation catalyzed by RT.[44,48] In our SM-PIFE studies, insights into the parameters pertaining to the binding kinetics and affinities of the three HIV-1 RT dimers were obtained by directly visualizing the binding/unbinding process. The SM-PIFE results demonstrate that the intrinsic binding affinities of RTp66−p51 and RTp66−p66 with their DNA−DNA substrates are 50−100-fold larger than that of RTp51−p51. The bound RTp51−p51/Cy3-P-T complex appears to be less stable (5−7 times bigger k_d) and highly dynamic, exhibiting faster binding/unbinding rates compared to RTp66−p51/Cy3-P-T or RTp66−p66/Cy3-P-T complexes.

It is well-known that the stability and the enzymatic activity of the three RT dimers exhibit a hierarchical order with RTp66−p51 > RTp66−p66 > RTp51−p51.[2,14,15,19] The SM-PIFE data presented here reveal that the initial binding of the three RT dimers to a DNA−DNA substrate also follows the same trend where heterodimeric RTp66−p51 has a slightly higher affinity than homodimeric RTp66−p66 and a much greater affinity than RTp51−p51. There exists a time-dependent decrease in the binding affinity of RT for its DNA substrate. While the binding events of either RTp66−p51 or RTp66−p66 with Cy3-P-T exhibited an appreciable but small reduction after 6 days, those of RTp51−p51 diminished within ca. 20 min. These data strongly support the notion that the dissociation of the RTp66−p51 heterodimer and the RTp66−p66 homodimer into their constituent monomers is significantly slower compared to that of RTp51−p51. The binding of both hetero- and homodimeric HIV-1 RT with their nucleic acid substrates is likely dominated by the protein dimerization process rather than by the intrinsic binding affinities of the functionally active dimeric forms.

■ ASSOCIATED CONTENT

Supporting Information

Detailed descriptions of fluorescence enhancement of Cy3-P-T induced by RT binding, steady fluorescence of Cy3-P-T in the absence of RT, electrophoretic mobility shift assay, on/off-time analysis, and determination of apparent dissociation constants by ensemble normalized intensity histograms. This material is available free of charge via the Internet at http://pubs.acs.org.

■ AUTHOR INFORMATION

Corresponding Author

*E-mail: gonzalo.cosa@mcgill.ca (G.C.); hsiao-wei.liu@mail.mcgill.ca (H.-W.L.); matthias.gotte@mcgill.ca (M.G.).

Author Contributions

H.-W.L. designed the research and established the experimental procedure and data analysis protocol. M.E. and C.J.A. expressed and purified proteins. R.A.M. performed the research and analyzed the data. H.-W.L. performed the measurement at high RT concentrations and analyzed the resulting data. H.-W.L. and R.A.M. prepared the manuscript draft. G.C. and M.G. designed and coordinated the study and revised the manuscript. All authors have given approval to the final version of the manuscript.

Notes

The authors declare no competing financial interest.

■ ACKNOWLEDGMENTS

G.C. and M.G. are thankful to the Fonds Québécois de la Recherche sur la Nature et les Technologies (FQRNT) Team Grant program, the National Science and Engineering Research Council of Canada (NSERC) (G.C.), the Canadian Institutes of Health Research (CIHR) (M.G.), and Nanoquebec (G.C.). M.G. is the recipient of a career award from the Fonds de la recherche en santé du Québec (FRSQ). H.-W.L. thanks both the McGill CIHR drug development training program (DDTP) and GRASP for a postdoctoral fellowship. R.A.M. thanks the previous two programs and the NSERC CREATE training program in bionanomachines for a postgraduate fellowship. C.J.A. is grateful for a DDTP postgraduate fellowship. M.E. is thankful to CIHR for a doctoral research award.

■ ABBREVIATIONS

HIV-1, human immunodeficiency virus type 1; RT, reverse transcriptase; SM-FRET, single-molecule fluorescence resonance energy transfer; SM-PIFE, single-molecule protein induced fluorescence enhancement; GST, glutathione S-transferase; PEG, poly(ethylene glycol); P-T, primer/template; TIRF, total internal reflection fluorescence; EM-CCD, electron multiplying charge coupled device; EMSA, electrophoretic mobility shift assay; RNase, ribonuclease; EFZ, efavirenz; NNRTI, non-nucleoside RT inhibitor

REFERENCES

(1) di Marzo Veronese, F.; Copeland, T. D.; DeVico, A. L.; Rahman, R.; Oroszlan, S.; Gallo, R. C.; Sarngadharan, M. G. *Science* **1986**, *231*, 1289−1291.
(2) Starnes, M. C.; Gao, W. Y.; Ting, R. Y.; Cheng, Y. C. *J. Biol. Chem.* **1988**, *263*, 5132−5134.
(3) Le Grice, S. F. J.; Naas, T.; Wohlgensinger, B.; Schatz, O. *EMBO J.* **1991**, *10*, 3905−3911.
(4) Kohlstaedt, L. A.; Wang, J.; Friedman, J. M.; Rice, P. A.; Steitz, T. A. *Science* **1992**, *256*, 1783−1790.
(5) Wang, J.; Smerdon, S. J.; Jager, J.; Kohlstaedt, L. A.; Rice, P. A.; Friedman, J. M.; Steitz, T. A. *Proc. Natl. Acad. Sci. U.S.A.* **1994**, *91*, 7242−7246.
(6) Hostomsky, Z.; Hostomska, Z.; Fu, T. B.; Taylor, J. *J. Virol.* **1992**, *66*, 3179−3182.
(7) Sluis-Cremer, N.; Arion, D.; Abram, M. E.; Parniak, M. A. *Int. J. Biochem. Cell Biol.* **2004**, *36*, 1836−1847.
(8) Ghosh, M.; Jacques, P. S.; Rodgers, D. W.; Ottman, M.; Darlix, J.-L.; Le Grice, S. F. J. *Biochemistry* **1996**, *35*, 8553−8562.
(9) Tachedjian, G.; Aronson, H.-E. G.; Goff, S. P. *Proc. Natl. Acad. Sci. U.S.A.* **2000**, *97*, 6334−6339.
(10) Wu, J.; Amandoron, E.; Li, X.; Wainberg, M. A.; Parniak, M. A. *J. Biol. Chem.* **1993**, *268*, 9980−9985.
(11) Müller, B.; Restle, T.; Weiss, S.; Gautel, M.; Sczakiel, G.; Goody, R. S. *J. Biol. Chem.* **1989**, *264*, 13975−13978.
(12) Le Grice, S. F. J.; Grüninger-Leitch, F. *Eur. J. Biochem.* **1990**, *187*, 307−314.
(13) Maier, G.; Dietrich, U.; Panhans, B.; Schröder, B.; Rübsamen-Waigmann, H.; Cellai, L.; Hermann, T.; Heumann, H. *Eur. J. Biochem.* **1999**, *261*, 10−18.
(14) Bavand, M. R.; Wagner, R.; Richmond, T. J. *Biochemistry* **1993**, *32*, 10543−10552.
(15) Fletcher, R. S.; Holleschak, G.; Nagy, E.; Arion, D.; Borkow, G.; Gu, Z.; Wainberg, M. A.; Parniak, M. A. *Protein Expression Purif.* **1996**, *7*, 27−32.
(16) El Dirani-Diab, R.; Andreola, M. L.; Nevinsky, G.; Tharaud, D.; Barr, P. J.; Litvak, S.; Tarrago-Litvak, L. *FEBS Lett.* **1992**, *301*, 23−28.
(17) Hansen, J.; Schulze, T.; Mellert, W.; Moelling, K. *EMBO J.* **1988**, *7*, 239−243.
(18) Hizi, A.; McGill, C.; Hughes, S. H. *Proc. Natl. Acad. Sci. U.S.A.* **1988**, *85*, 1218−1222.
(19) Restle, T.; Müller, B.; Goody, R. S. *J. Biol. Chem.* **1990**, *265*, 8986−8988.
(20) Tisdale, M.; Ertl, P.; Larder, B. A.; Purifoy, D. J.; Darby, G.; Powell, K. L. *J. Virol.* **1988**, *62*, 3662−3667.
(21) Liu, H.-W.; Zeng, Y.; Landes, C. F.; Kim, Y. J.; Zhu, Y.; Ma, X.; Vo, M.-N.; Musier-Forsyth, K.; Barbara, P. F. *Proc. Natl. Acad. Sci. U.S.A.* **2007**, *104*, 5261−5267.
(22) Cosa, G.; Harbron, E. J.; Zeng, Y.; Liu, H.-W.; O Connor, D. B.; Eta-Hosokawa, C.; Musier-Forsyth, K.; Barbara, P. F. *Biophys. J.* **2004**, *87*, 2759−2767.
(23) Berezhna, S. Y.; Gill, J.; Lamichhane, R.; Millar, D. P. *J. Am. Chem. Soc.* **2012**, *134*, 11261−11268.
(24) Abbondanzieri, E. A.; Bokinsky, G.; Rausch, J. W.; Zhang, J. X.; Le Grice, S. F. J.; Zhuang, X. *Nature* **2008**, *453*, 184−189.
(25) Christian, T. D.; Romano, L. J.; Rueda, D. *Proc. Natl. Acad. Sci. U.S.A.* **2009**, *106*, 21109−21114.
(26) Myong, S.; Rasnik, I.; Joo, C.; Lohman, T. M.; Ha, T. *Nature* **2005**, *437*, 1321−1325.
(27) Rasnik, I.; Myong, S.; Cheng, W.; Lohman, T. M.; Ha, T. *J. Mol. Biol.* **2004**, *336*, 395−408.
(28) Joo, C.; McKinney, S. A.; Nakamura, M.; Rasnik, I.; Myong, S.; Ha, T. *Cell* **2006**, *126*, 515−527.
(29) Hwang, H.; Kim, H.; Myong, S. *Proc. Natl. Acad. Sci. U.S.A.* **2011**, *108*, 7414−7418.
(30) Luo, G.; Wang, M.; Konigsberg, W. H.; Xie, X. S. *Proc. Natl. Acad. Sci. U.S.A.* **2007**, *104*, 12610−12615.
(31) Ngo, A. T.; Karam, P.; Fuller, E.; Burger, M.; Cosa, G. *J. Am. Chem. Soc.* **2007**, *130*, 457−459.
(32) Karam, P.; Ngo, A. T.; Rouiller, I.; Cosa, G. *Proc. Natl. Acad. Sci. U.S.A.* **2010**, *107*, 17480−17485.
(33) Liu, H.-W.; Ngo, A. T.; Cosa, G. *J. Am. Chem. Soc.* **2011**, *134*, 1648−1652.
(34) Ding, J.; Das, K.; Hsiou, Y.; Sarafianos, S. G.; Clark, A. D., Jr.; Jacobo-Molina, A.; Tantillo, C.; Hughes, S. H.; Arnold, E. *J. Mol. Biol.* **1998**, *284*, 1095−1111.
(35) Debyser, Z.; De Clercq, E. *Protein Sci.* **1996**, *5*, 278−286.
(36) We note that an additional bright state may be present in our single molecule data, reflecting dynamics of the p66 fingers domain (i.e., closing over the 3′OH of the primer, as reported in ref 28).
(37) McKinney, S. A.; Joo, C.; Ha, T. *Biophys. J.* **2006**, *91*, 1941−1951.
(38) Kruhøfter, M.; Urbanke, C.; Grosse, F. *Nucleic Acids Res.* **1993**, *21*, 3943−3949.
(39) Levitus, M.; Ranjit, S. *Q. Rev. Biophys.* **2011**, *44*, 123−151.
(40) Götte, M.; Maier, G.; Onori, A. M.; Cellai, L.; Wainberg, M. A.; Heumann, H. *J. Biol. Chem.* **1999**, *274*, 11159−11169.
(41) Biondi, M. J.; Beilhartz, G. L.; McCormick, S.; Götte, M. *J. Biol. Chem.* **2010**, *285*, 26966−26975.
(42) Venezia, C. F.; Howard, K. J.; Ignatov, M. E.; Holladay, L. A.; Barkley, M. D. *Biochemistry* **2006**, *45*, 2779−2789.
(43) Venezia, C. F.; Meany, B. J.; Braz, V. A.; Barkley, M. D. *Biochemistry* **2009**, *48*, 9084−9093.
(44) DeStefano, J. J.; Bambara, R. A.; Fay, P. J. *Biochemistry* **1993**, *32*, 6908−6915.
(45) Kati, W. M.; Johnson, K. A.; Jerva, L. F.; Anderson, K. S. *J. Biol. Chem.* **1992**, *267*, 25988−25997.
(46) Zheng, X.; Mueller, G. A.; Cuneo, M. J.; DeRose, E. F.; London, R. E. *Biochemistry* **2010**, *49*, 2821−2833.
(47) Ignatov, M. E.; Berdis, A. J.; Le Grice, S. F. J.; Barkley, M. D. *Biochemistry* **2005**, *44*, 5346−5356.
(48) Bohlayer, W. P.; DeStefano, J. J. *Biochemistry* **2006**, *45*, 7628−7638.
(49) Reardon, J. E. *J. Biol. Chem.* **1993**, *268*, 8743−8751.